Optimization, tolerance analysis and implementation of a Stokes polarimeter based on the conical refraction phenomenon

Alba Peinado,[1,*] Angel Lizana,[1] Alejandro Turpín,[1] Claudio Iemmi,[2] Todor K. Kalkandjiev,[1] Jordi Mompart,[1] and Juan Campos[1]

[1]*Departament de Física, Universitat Autònoma de Barcelona, 08193 Bellaterra, Spain.*
[2]*Departamento de Física, FCEN, Universidad de Buenos Aires, 1428 Buenos Aires, Argentina.*
[*]*alba.peinado@uab.es*

Abstract: Recently, we introduced the basic concepts behind a new polarimeter device based on conical refraction (CR), which presents several appealing features compared to standard polarimeters. To name some of them, CR polarimeters retrieve the polarization state of an input light beam with a snapshot measurement, allow for substantially enhancing the data redundancy without increasing the measuring time, and avoid instrumental errors owing to rotating elements or phase-to-voltage calibration typical from dynamic devices. In this article, we present a comprehensive study of the optimization, robustness and parameters tolerance of CR based polarimeters. In addition, a particular CR based polarimetric architecture is experimentally implemented, and some concerns and recommendations are provided. Finally, the implemented polarimeter is experimentally tested by measuring different states of polarization, including fully and partially polarized light.

OCIS codes: (120.5410) Polarimetry; (120.2130) Ellipsometry and polarimetry; (260.5430) Polarization; (260.1440) Birefringence.

References and links

1. R. M. A. Azzam and N. M. Bashara, *Ellipsometry and Polarized Light* (North-Holland Publishing Company, 1977).
2. V. A. Escobar, J. R. Rangel, N. V. Pérez, G. Andrade, and J. L. Dávila, *Infrared Spectroscopy – Materials Sciencie, Enginneering and Technology* (Intech, 2012), Chap. 9.
3. N. L. Do, E. Garcia-Caurel, N. Bererd, N. Moncoffre, and D. Gorse-Pomonti, "Determination of thicknesses of oxide films grown on titanium under argon irradiation by spectroscopic ellipsometry," J. Nucl. Mater. **447**(1–3), 197–207 (2014).
4. A. Lizana, M. Foldyna, M. Stchakovsky, B. Georges, N. David, and E. Garcia-Caurel, "Enhanced sensitivity to dielectric function and thickness of absorbing thin film by combining total internal reflection ellipsometry with standard ellipsometry and reflectometry," J. Phys. D Appl. Phys. **46**(10), 105501 (2013).
5. K. M. Twietmeyer, R. A. Chipman, A. E. Elsner, Y. Zhao, and D. VanNasdale, "Mueller matrix retinal imager with optimized polarization conditions," Opt. Express **16**(26), 21339–21354 (2008).
6. M. R. Antonelli, A. Pierangelo, T. Novikova, P. Validire, A. Benali, B. Gayet, and A. De Martino, "Mueller matrix imaging of human colon tissue for cancer diagnostics: how Monte Carlo modeling can help in the interpretation of experimental data," Opt. Express **18**(10), 10200–10208 (2010).
7. N. Uribe-Patarroyo, A. Alvarez-Herrero, R. L. Heredero, J. C. del Toro, A. C. López, V. Domingo, J. L. Gasent, L. Jochum, and V. Martínez, "IMaX: a polarimeter based on liquid crystal variable retarders for an aerospace mission," Phys. Status Solidi C **5**(5), 1041–1045 (2008).
8. D. F. Elmore, B. W. Lites, S. Tomczyk, A. Skumanich, R. B. Dunn, J. A. Schuenke, K. V. Streander, T. W. Leach, C. W. Chambellan, H. K. Hull, and L. B. Lacey, "Advanced Stokes polarimeter: a new instrument for solar magnetic field research," Proc. SPIE **1746**, 138795 (1992).
9. R. A. Chipman, "Polarimetry," *in Handbook of Optics*, M. Bass, ed. (McGraw-Hill, 1995).
10. J. S. Tyo, D. L. Goldstein, D. B. Chenault, and J. A. Shaw, "Review of passive imaging polarimetry for remote sensing applications," Appl. Opt. **45**(22), 5453–5469 (2006).

#224967 - $15.00 USD Received 17 Oct 2014; revised 11 Jan 2015; accepted 12 Jan 2015; published 24 Feb 2015

11. A. Peinado, A. Lizana, J. Vidal, C. Iemmi, and J. Campos, "Optimization and performance criteria of a Stokes polarimeter based on two variable retarders," Opt. Express **18**(10), 9815–9830 (2010).
12. D. S. Sabatke, M. R. Descour, E. L. Dereniak, W. C. Sweatt, S. A. Kemme, and G. S. Phipps, "Optimization of retardance for a complete Stokes polarimeter," Opt. Lett. **25**(11), 802–804 (2000).
13. J. L. Pezzaniti and R. A. Chipman, "Mueller matrix imaging polarimetry," Opt. Eng. **34**(6), 1558–1568 (1995).
14. P. Raman, K. Fuller, D. Gregory, M. Newchurch, and J. Christy, "Broadband (UV-VIS-NIR) Mueller matrix polarimeter," Proc. SPIE **8160**, 816013 (2011).
15. S. Savenkova, R. Muttiahb, E. Oberemoka, and A. Klimova, "Incomplete active polarimetry: Measurement of the block-diagonal scattering matrix," J. of Quant. Spec. and Rad. Trans. **112**(11), 1796–1802 (2011).
16. E. Garcia-Caurel, A. De Martino, and B. Drevillon, "Spectroscopic Mueller polarimeter based on liquid crystal devices," J. Thin Solid Films **455–456**, 120–123 (2004).
17. L. Gendre, A. Foulonneau, and L. Bigué, "Imaging linear polarimetry using a single ferroelectric liquid crystal modulator," Appl. Opt. **49**(25), 4687–4699 (2010).
18. A. Peinado, A. Lizana, J. Vidal, C. Iemmi, and J. Campos, "Optimized Stokes polarimeters based on a single twisted nematic liquid-crystal device for the minimization of noise propagation," Appl. Opt. **50**(28), 5437–5445 (2011).
19. E. Compain and B. Drevillon, "Broadband division-of-amplitude polarimeter based on uncoated prisms," Appl. Opt. **37**(25), 5938–5944 (1998).
20. A. Peinado, A. Turpin, A. Lizana, E. Fernández, J. Mompart, and J. Campos, "A method for polarization metrology based on the conical refraction," Opt. Lett. **38**(20), 4100–4103 (2013).
21. J. L. Pezzaniti and D. B. Chenault, "A division of aperture MWIR imaging polarimeter," Proc. SPIE **5888**, 58880V (2005).
22. M. V. Berry and M. R. Jeffrey, "Conical diffraction: Hamilton's diabolical point at the heart of crystal optics," Prog. Opt. **50**, 13–50 (2007).
23. A. M. Belskii and A. P. Khapalyuk, "Internal conical refraction of bounded light beams in biaxial crystals," Opt. Spectrosc. **44**, 436–439 (1978).
24. T. K. Kalkandjiev and M. A. Bursukova, "Conical refraction: an experimental introduction," Proc. SPIE **6994**, 69940B (2008).
25. A. Turpin, Y. V. Loiko, T. K. Kalkandjiev, H. Tomizawa, and J. Mompart, "Wave-vector and polarization dependence of conical refraction," Opt. Express **21**(4), 4503–4511 (2013).
26. A. Turpin, Y. V. Loiko, T. K. Kalkandjiev, and J. Mompart, "Multiple rings formation in cascaded conical refraction," Opt. Lett. **38**(9), 1455–1457 (2013).
27. A. Turpin, Y. Loiko, T. K. Kalkandjiev, and J. Mompart, "Free-space optical polarization demultiplexing and multiplexing by means of conical refraction," Opt. Lett. **37**(20), 4197–4199 (2012).
28. Y. V. Loiko, G. S. Sokolovskii, D. Carnegie, A. Turpin, J. Mompart, and E. U. Rafailov, "Laser beams with conical refraction patterns," Proc. SPIE **8960**, 89601Q (2014).
29. D. P. O'Dwyer, C. F. Phelan, K. E. Ballantine, Y. P. Rakovich, J. G. Lunney, and J. F. Donegan, "Conical diffraction of linearly polarized light controls the angular position of a microscopic object," Opt. Exp. **18**(26), 27319–27326 (2010).
30. P. Taylor, *Theory and Applications of Numerical Analysis* (Academic, 1996).
31. J. S. Tyo, "Design of optimal polarimeters: maximization of signal-to-noise ratio and minimization of systematic error," Appl. Opt. **41**(4), 619–630 (2002).
32. F. Goudail, "Noise minimization and equalization for Stokes polarimeters in the presence of signal-dependent Poisson shot noise," Opt. Lett. **34**(5), 647–649 (2009).
33. D. Lara and C. Paterson, "Stokes polarimeter optimization in the presence of shot and Gaussian noise," Opt. Express **17**(23), 21240–21249 (2009).
34. G. Anna and F. Goudail, "Optimal Mueller matrix estimation in the presence of Poisson shot noise," Opt. Express **20**(19), 21331–21340 (2012).
35. D. S. Sabatke, A. M. Locke, M. R. Descour, W. C. Sweatt, J. P. Garcia, E. L. Dereniak, S. A. Kemme, and G. S. Phipps, "Figures of merit for complete Stokes polarimeter optimization," Proc. SPIE **4133**, 75–81 (2000).
36. E. Chironi and C. Iemmi, "Bounding the relative errors associated with a complete Stokes polarimeter," J. Opt. Soc. Am. A **31**(1), 75–80 (2014).
37. A. Peinado, A. Lizana, and J. Campos, "Optimization and tolerance analysis of a polarimeter with ferroelectric liquid crystals," Appl. Opt. **52**(23), 5748–5757 (2013).
38. J. C. Kemp and M. S. Barbour, "A photoelastic-modulator polarimeter at Pine Mountain Observatory," Publ. Astron. Soc. Pac. **93**, 521–525 (1981).
39. O. Arteaga, J. Freudenthal, B. Wang, and B. Kahr, "Mueller matrix polarimetry with four photoelastic modulators: theory and calibration," Appl. Opt. **51**(28), 6805–6817 (2012).
40. G. Goldstein, *Polarized Light* (Marcel Dekker, 2003).
41. R. M. A. Azzam, I. M. Elminyawi, and A. M. El-Saba, "General analysis and optimization of the four-detector photopolarimeter," J. Opt. Soc. Am. A **5**(5), 681–689 (1988).
42. A. De Martino, Y. K. Kim, E. Garcia-Caurel, B. Laude, and B. Drévillon, "Optimized Mueller polarimeter with liquid crystals," Opt. Lett. **28**(8), 616–618 (2003).

#224967 - $15.00 USD Received 17 Oct 2014; revised 11 Jan 2015; accepted 12 Jan 2015; published 24 Feb 2015

43. L. Neumann, R. Hegedus, G. Horvath, and R. Garcia, "Applications for high precision imaging polarimetry," in Proceedings of the Fourth Eurographics conference on Computational Aesthetics in Graphics, Visualization and Imaging (Eurographics Association, 2008), pp.89–97.
44. E. Compain, S. Poirier, and B. Drevillon, "General and self-consistent method for the calibration of polarization modulators, polarimeters, and mueller-matrix ellipsometers," Appl. Opt. **38**(16), 3490–3502 (1999).
45. S. Huard, *Polarisation de la lumière* (Masson, 1994).
46. S.-Y. Lu and R. A. Chipman, "Interpretation of Mueller matrices based on polar decomposition," J. Opt. Soc. Am. A **13**(5), 1106–1113 (1996).
47. T. K. Kalkandjiev and M. A. Bursukova, "Conical refraction: an experimental introduction," Proc. SPIE **6994**, 69940B (2008).
48. M. H. Smith, J. B. Woodruff, and J. D. Howe, "Beam wander considerations in imaging polarimetry," Proc. SPIE **3754**, 50–54 (1999).
49. A. Peinado, A. Lizana, and J. Campos, "Use of ferroelectric liquid crystal panels to control state and degree of polarization in light beams," Opt. Lett. **39**(3), 659–662 (2014).

1. Introduction

There are numerous fields where the accurate knowledge of the polarization of a given light beam or of the polarimetric properties of a certain material becomes relevant. For instance, polarimetric information is currently used in a widespread number of different optical applications, as for instance, for the characterization of the optical parameters (index of refraction, thickness, absorption coefficient, roughness, etc.) of materials structured in thin films [1–4], for medical imaging [5,6], or in astronomy [7,8], among many others.

Polarimeters are the main devices to perform polarimetric measurements. Different architectures have been proposed, leading to different performances with strengths and weaknesses in terms of their metrological capabilities. Polarimeters can be grouped in different classes according to some of their main features [9,10]. For instance, Stokes polarimeters [11,12] are able to measure the State of Polarization (SoP) of a light beam while Mueller polarimeters [13,14] are able to determine the polarimetric properties of a polarimetric sample. An alternative classification can be established as a function of their completeness when performing polarimetric measurements [11,15]. Thus, an incomplete polarimeter is able to provide partial polarimetric information of a light beam or a sample, whereas a complete polarimeter provides the full polarimetric content. Finally, by analyzing the operational properties of the optical elements used to build up the polarimeters, they can be grouped as mechanical polarimeters [12,13], dynamic polarimeters [11,16–18] or static polarimeters [19–21]. Whereas the two formers require of mechanical rotations of the elements or some kind of electrical addressing to carry out the measurements (they are time-sequential polarimeters), the static polarimeters are able to instantaneously measure the polarimetric information. This last group is usually formed by polarimeters based on aperture-division or amplitude-division set-ups, so they lead to a certain decrease of the signal-to-noise ratio, when compared with the performance of sequential polarimeters operating with a light source of the same power.

A new tool for polarization metrology, based on the Conical Refraction (CR) phenomenon [22–29], was recently presented in [20]. CR refers to the propagation of a collimated light beam along one of the optic axes of a biaxial crystal to emerge as a hollow cylinder. Each two opposite points of the ring transverse intensity pattern have orthogonal linear polarizations, which indicates that the ring intensity distribution behaves as a full projection of the input beam polarization. Thus, both circularly polarized and fully unpolarized input light give rise to a uniform ring intensity distribution, while linearly polarized input light yields a crescent intensity distribution with one point of null intensity. Taking advantage of the CR phenomenon, an amplitude-division polarimeter, resulting in a complete punctual Stokes polarimeter, was presented in [20]. This new optical device, which includes two biaxial crystals, allowed measuring any SoP of the input light beam by analyzing the mapping that the CR phenomenon produces between the polarization of the input beam and the transverse intensity distribution along the ring of the output beam [22]. This new architecture allows the system to define a set of polarization analyzers (*i.e.*, different SoPs where the input

#224967 - $15.00 USD Received 17 Oct 2014; revised 11 Jan 2015; accepted 12 Jan 2015; published 24 Feb 2015

polarization is projected) by neither using mechanical movements of its optical elements nor applying electrical addressing (as it is the case of liquid crystal based polarimeters [11,16–18]). Therefore, the CR polarimeter becomes appealing for optical applications not only because it avoids experimental errors related to misalignments or to experimental deviations of the phase-voltage look-up table, but also because its static performance permits to completely determine the SoP of a light beam by achieving a measure almost instantaneous (only limited by the acquisition time and the software computation time). In addition, as it is shown in this paper, this architecture also allows to easily increasing the number of polarization analyzers just by selecting a larger number of points over the intensity distribution ring produced by the conical refraction phenomenon. Thus, the number of polarization analyzers used is only limited by the geometrical characteristics of the camera pixel array. Therefore, the data redundancy of the system can be easily increased, leading to a reduction for the experimental measurement variance values, without requiring an increase of the measuring time.

The concept of using the CR phenomenon as a tool for polarization metrology and an experimental validation of their potential for polarimetric applications were provided in [20]. However, neither specific details of the CR polarimeter experimental implementation and testing, nor an evaluation of its optimized performance or its accuracy and robustness to perform polarimetric measurements, were included. We consider that this information is crucial to those users interested in using CR based polarimeters for their current polarimetric applications. Therefore, in this paper we attempt to complete the study provided in [20], by applying a general methodology to evaluate the tolerance and robustness performance of polarimeters to the particular architecture which is based on the CR phenomenon. A comprehensive description of the procedure used during the experimental implementation and calibration of the CR polarimeter prototype is provided, and an analysis of the obtained results is included.

The outline of this paper is as follows. In section 2, a review of the measurement principle for polarimeters as well as a summary of certain quality indicators, useful to optimize the polarimeters performance in terms of noise propagation, are provided. In section 3, the CR polarimeter architecture implemented in this work is presented and a study of its optimized performance is performed. In section 4, a thoroughly analysis of the robustness and the parameters tolerance is given. In addition, detailed descriptions of the CR polarimeter implementation, as well as an analysis of the polarimetric metrology capability, are provided in section 5. Finally, last section summarizes the main conclusions obtained from this work.

2. Polarimeter fundamentals

In this section, some significant concepts, essential for the development of the Conical Refraction (CR) polarimeter, are reviewed. First, the measurement principle of polarimeters is here provided. In addition, a brief examination of different quality indicators, able to estimate the polarimeters performance in terms of noise propagation, is also provided. Finally, a methodology able to determine the tolerance of the parameters involved in the polarimeter architecture is described. All this information is a crucial knowledge insofar as it is applied in the following sections, for the proper implementation of the CR polarimeter measuring procedure as well as to ensure its optimized performance.

To describe the measurement principle for a Stokes polarimeter, let us represent the polarimetric system matrix A, by a nx4 matrix containing (arranged in rows) the n different Polarization Analyzers (PAs) proper of a given polarimeter. Note that these PAs are different states of polarization evaluating the polarimetric content of an incident light beam, and they are completely defined by the diverse configurations of a particular Polarization State Analyzer (PSA) [9]. In this situation, by projecting an incident state of polarization, described by a Stokes vector S, on the different PAs arranged into the matrix A, an nx1 flux vector I is

#224967 - $15.00 USD Received 17 Oct 2014; revised 11 Jan 2015; accepted 12 Jan 2015; published 24 Feb 2015

obtained at the exit of the system. This situation is mathematically described by the following linear relation:

$$I = A \cdot S. \tag{1}$$

If the polarimetric system matrix A is well calibrated, an unknown SoP can be determined by inverting Eq. (1),

$$S = A^{-1} \cdot I = Q \cdot I \Rightarrow S_i = \sum_{j=1}^{n} \left(q_{i,j} \cdot I_j \right), \tag{2}$$

where Q is the polarimetric data reduction matrix (*i.e.*, the inverse, or the pseudo-inverse [9] for non-squared matrices, of the matrix A) and the different $q_{i,j}$ are its coefficients. The indicator n accounts for the number of PAs present into the matrix A, and the counters i and j are integer numbers which take their values from the sets $i = \{0,1,2,3\}$ and $j = \{1,...,n\}$, respectively.

At this point, if the polarimetric system matrix A is a non-singular matrix and it is well-calibrated, by performing radiometric measurements of the flux vector I, the Stokes elements of an incident light beam can be readily and completely determined by following Eq. (2). Given a particular PSA related to certain polarimeter architecture, the construction of the polarimetric system matrix A is not unique. In fact, by arranging different PAs subsets from the entire set of available PAs, an infinite number of non-singular matrices A can be built-up. However, the conditioning [30] of these matrices will be different, and thus, the amplification of the experimental noise from the flux vector I to the final Stokes vector measurement, due to the matrix inversion in Eq. (2), will be different as well.

To optimize the performance of polarimeters in terms of noise amplification, different quality indicators are provided and discussed in the literature [11, 12, 31–36]. A commonly used quality indicator in polarimetry is the Condition Number (CN) [30]. This parameter, defined as the ratio of the largest over the smallest singular values of the evaluated matrix, allows us to minimize the amplification of errors from the raw-data to the computed Stokes vector by estimating how far the system matrix A is from singularity.

Therefore, an optimized performance of the polarimeter can be achieved by taking into account the CN criterion. In addition, if we are also interested in the specific noise propagated to each coefficient of the Stokes vector, the error propagated through Eq. (2) can be calculated. This is conducted by considering that the noise at the j components of the flux vector I are not correlated between them, and uniformly distributed ($\delta I_j = \delta I$). In such case, by considering Eq. (2), the variances of the Stokes elements can be written as follows [11, 12]:

$$\delta S_i^2 = \sum_{j=1}^{n} \left(\frac{\partial S_i}{\partial I_j} \right)^2 \cdot \delta I_j^2 = \delta I^2 \sum_{j=1}^{n} q_{i,j}^2, \tag{3}$$

Alternatively, we want to underline another quality indicator widespread used in polarimetry, the so-called Equally Weighted Variance (EWV) [11, 12]. This indicator is particularly of interest when all the different Stokes components variances are equally of interest and it can be calculated as the addition, with equal weights, of the four Stokes element variances (deduced from Eq. (3)).

Finally, a methodology able to estimate the parameters tolerance for polarimeter architectures in order to ensure a given accuracy is reviewed [37]. Let us suppose that the actual polarimetric system matrix A_{exp} is slightly different from the calibrated one, labeled as A. Note that these differences always exist due to multiple experimental factors. By taking into account Eq. (2), the estimated Stokes vector S_{est} is related to the actual Stokes vector S as follows [37]:

#224967 - $15.00 USD Received 17 Oct 2014; revised 11 Jan 2015; accepted 12 Jan 2015; published 24 Feb 2015

$$S_{est} = A^{-1} \cdot A_{\exp} \cdot S, \tag{4}$$

Note that in the ideal case where $A = A_{exp}$, the estimated Stokes vector S_{est} is exactly the actual one. In general, there is always a difference (error e_s) between the estimated Stokes vector S_{est} and the actual one S, which can be expressed, by taking into account Eq. (4), in the following form:

$$e_s = S - S_{est} = \left(Id - A^{-1} \cdot A_{\exp} \right) \cdot S, \tag{5}$$

where *Id* accounts for the identity matrix. Note that Eq. (5) can be readily extended to non-squared matrices just by including the concept of pseudo-inverse matrix [9].

3. CR polarimeter architecture and evaluation of its optimized performance

As stated before, the experimental implementation of a punctual and complete Stokes polarimeter based on the Conical Refraction (CR) phenomenon is presented in this paper. The CR polarimeter architecture chosen to be experimentally implemented is the one suggested in [20]. In this section, a brief description of this CR polarimeter architecture and an optimization of its performance are provided.

3.1 Conical Refraction polarimeter architecture

The CR polarimeter architecture used in this work is sketched in Fig. 1. The system is illuminated with light beam with unknown SoP. By means of a beam-splitter, the studied light beam is split in two beams which are analyzed separately by two different polarizing analyzer arms, labeled as arm 1 and arm 2 respectively. Both analyzing arms include a biaxial crystal, which were cut with one of the optic axes perpendicular to the slab faces. Under this scenario, when an incident beam enters perpendicular to one of the lateral faces of the biaxial crystal, the CR phenomenon occurs [22, 24–26]. This situation is ensured by means of the Lens 0 (see Fig. 1), which focuses the input beam into the two biaxial crystals and perpendicularly to their slab faces. Under these conditions, the light beam passing along the optical axis of each biaxial crystal forms at the Lens 0 focal plane (planes P_1 and P_2 respectively) the corresponding intensity distribution (*i.e.*, the CR ring) described in Refs [20, 24]. Finally, the lenses Lens 1 and Lens 2 image the CR rings at the corresponding CCD camera planes, with a certain magnification.

Note that there is a link between the polarization of the input beam at the entrance of the biaxial crystal and the transverse intensity distribution along the CR intensity ring of the output beam. In fact, the pass of the incident light through a biaxial crystal can be described as the projection of the input beam into an infinite number of linearly polarized states arranged in a circle [20]. Moreover, the orientation of the transmission axis of those equivalent polarizers is spatially rotated from 0° to 180° along the circle. Thus, by using this property, an infinite set of linear Polarization Analyzers (PAs) is defined at the exit of the arm 1.

Finally, we want to note that the optical elements and their disposition into the set-up sketched in Fig. 1 are identical for both arms 1 and 2, except for the inclusion of a waveplate (WP) before the biaxial crystal at arm 2. This optical element (and the whole arm 2) is necessary to determine the ellipticity information of the input state polarization, which is not available from the arm 1 all alone. In fact, by including the WP in arm 2, the intensity pattern at plane P_2 can be understood as the result of projecting the incident beam over a WP and then, over the set of rotated polarizers arranged in a circle.

#224967 - $15.00 USD Received 17 Oct 2014; revised 11 Jan 2015; accepted 12 Jan 2015; published 24 Feb 2015

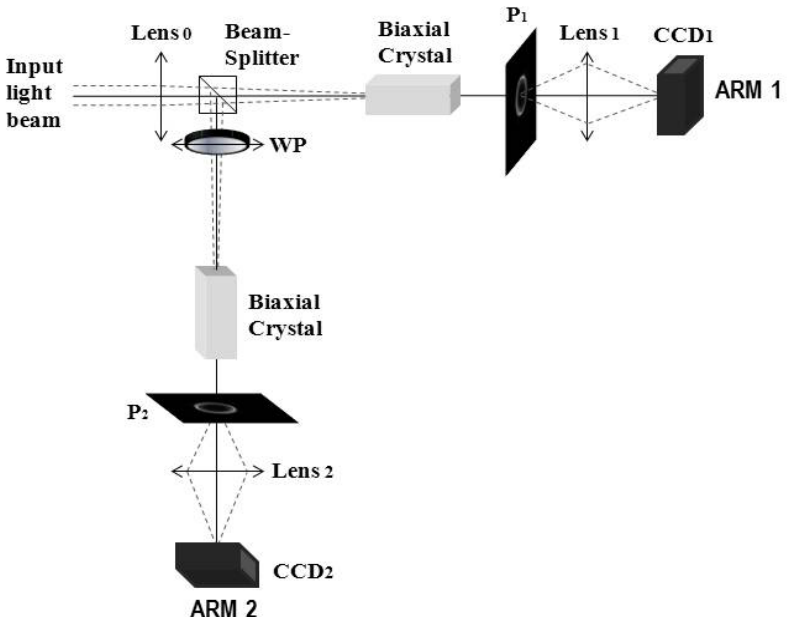

Fig. 1. Set-up of the polarimeter based on two biaxial crystals. The incident light beam is divided in two arms for being separately analyzed.

3.2 CR polarimeter optimized performance

Most Stokes polarimeters proposed in the literature generate the required Polarization Analyzers (PAs) by means of different configurations of the optical elements into their Polarization State Analyzer (PSA) systems. For instance, in certain polarimeters the different PAs are obtained by performing rotations of polarizers or retarders (linear waveplates, Fresnel bi-rhombs, etc [4, 12, 13], whilst in other polarimeters the set of different PSAs are achieved by generating different phases by means of dynamic elements as can be Liquid Crystal (LC) panels [11, 16–18, 37] or Photo-Elastic (PE) modulators [38, 39]. In all the cases, to ensure an accurate performance of the polarimeters, an optimization procedure of the optical parameters present in the system (orientations, retardances, etc.) must be conducted [11, 12, 18, 31–37].

Unlike the above-stated polarimeter architectures, the CR polarimeter generates the different PAs due to the CR phenomenon produced at the biaxial crystals (see Fig. 1). Thus, it results in a one-shot static polarimeter, where all the optical elements constituting the set-up are static. In addition, the only optical parameters that may vary the Condition Number (CN), so susceptible to be optimized, are the orientation and the retardance of the WP in arm 2.

Under this scenario, the optimal orientation and retardance for the WP, in terms of noise amplification, must be studied. To this aim, an optical model describing the CR polarimeter performance is developed in this section. From the Mueller-Stokes formalism [9, 40], the different PAs available with the CR polarimeter are determined by the first row of the Mueller matrices describing the analyzer arms 1 and 2, respectively. In particular, the arm 1 available PAs are described by the first row of the Mueller matrix of a linear polarizer with the transmission axis orientated at an angle θ_{LP} (being the angular position of the particular PAs at the ring equal to $2\theta_{LP}$). Similarly, arm 2 available PAs are described by the first row of a Mueller matrix obtained by multiplying the Mueller matrix of a linear retarder (oriented at an angle θ_{WP} and with a retardance of δ) by the Mueller matrix of a linear polarizer with the transmission axis orientated at an angle θ_{LP}. They can be expressed as follows:

$$PA_1(\theta_{LP}) = \frac{1}{2}\begin{pmatrix} 1 & \cos 2\theta_{LP} & \sin 2\theta_{LP} & 0 \end{pmatrix}, \tag{6}$$

#224967 - $15.00 USD Received 17 Oct 2014; revised 11 Jan 2015; accepted 12 Jan 2015; published 24 Feb 2015

$$PA_2(\theta_{LP},\theta_{WP},\delta)=\frac{1}{2}(1 \quad p_1 \quad p_2 \quad p_3), \tag{7}$$

where

$$\begin{cases} p_1=\cos 2\theta_{LP}\left[\cos^2 2\theta_{WP}+\cos\delta\sin^2 2\theta_{WP}\right]+\sin 2\theta_{LP}\left[(1-\cos\delta)\sin 2\theta_{WP}\cos 2\theta_{WP}\right], \\ P_2=\cos 2\theta_{LP}\left[(1-\cos\delta)\sin 2\theta_{WP}\cos 2\theta_{WP}\right]+\sin 2\theta_{LP}\left[\sin^2 2\theta_{WP}+\cos\delta\cos^2 2\theta_{WP}\right], \\ P_3=\cos 2\theta_{LP}\left[\sin\delta\sin 2\theta_{WP}\right]-\sin 2\theta_{LP}\left[\sin\delta\cos 2\theta_{WP}\right]. \end{cases} \tag{8}$$

Note that the intensity distribution measured by the cameras CCD_1 and CCD_2 is the projection of the incident Stokes vector over the PAs described by Eqs. (6) and (7). Once the set of PAs available from the CR polarimeter is determined, an optimization of the system must be carried out. First, to obtain some visual insight on the CR polarimeter performance, the available PAs for arm 1 (red circle) and arm 2 (blue circle) are represented with steps of 0.5 degree for the θ_{LP} parameter (*i.e.*, 360 PAs per arm) upon the Poincaré sphere depicted in Fig. 2.

As previously stated, the PAs related to the arm 1 (Eq. (6)) cannot be optimized, as they are completely defined by the CR phenomenon. However, the set of PAs related to the arm 2 (Eq. (7)) depends on the selected WP retardance δ and orientation θ_{WP}. To illustrate this fact, Fig. 2(a) shows the PAs over the Poincare sphere for different values of the retardance δ (*i.e.*, $\delta=\{10,50,90,130,170\}$) and with θ_{WP} fixed to 0 degrees, which results in different rotations of the blue circle about the *S1* axis. In turn, Fig. 2(b) shows an analogous representation but for the PAs related to different values of θ_{WP} (*i.e.*, $\theta_{WP}=\{0,22.5,45,67.5,90\}$), when fixing δ to 90 degrees, which results in different rotations of the blue circle about the *S3* axis.

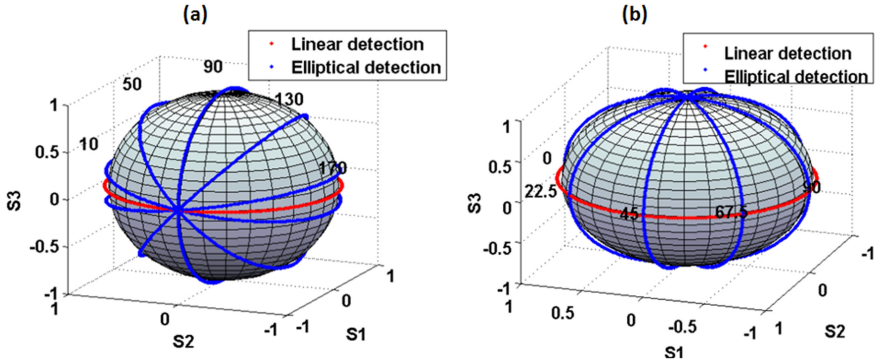

Fig. 2. CR polarimeter PAs represented over the Poincaré sphere for the arm 1 (in red) and the arm 2 (in blue) and for different values of: (a) the WP retardance (with θ_{WP} = 0 degrees); (b) the WP orientation (with δ = 90 degrees).

As argued in literature [10–12, 41], the larger the volume enclosed at the Poincaré sphere by the PAs related to a certain polarimeter, the better the conditioning of the system. By analyzing the volume enclosed by the PAs related to the analyzer arm 1 (red circle) and the analyzer arm 2 (blue circle) (Figs. 2(a) and 2(b)), some conclusions can be extracted. In particular, Fig. 2(a) shows that the volume enclosed at the Poincaré sphere strongly depends on the WP retardance. In fact, the largest volume is obtained by the blue circle related to the retardance of 90 degrees, leading to the best possible conditioning. Regarding to Fig. 2(b), it shows that the volume enclosed at the Poincaré sphere is constant, independently of the WP orientation chosen. Thus, the conditioning of the system is independent of this parameter. This result is logical by taking into account the symmetry exhibited by the CR ring polarization spatial distribution.

#224967 - $15.00 USD Received 17 Oct 2014; revised 11 Jan 2015; accepted 12 Jan 2015; published 24 Feb 2015

The results shown in Fig. 2 are in agreement with those obtained quantitatively by calculating the CN number [30] of different polarimetric system matrices A, which are built from diverse sets of PAs related to different WP orientations and retardances. The obtained results are shown in Fig. 3. Whereas Fig. 3(a) shows the CN as a function of different retardances of the WP (and constant $\theta_{WP} = 0°$), Fig. 3(b) shows the same indicator but as a function of different orientations of the WP (and constant $\delta = 90°$). Figure 3(a) verifies that the CN strongly depends on the WP retardance, reaching a minimum value for a retardance of 90 degrees. In addition, Fig. 3(b) provides that the CN is constant as a function of the WP orientation. To obtain the results given in Fig. 3(b), the WP retardance is fixed to 90 degrees, as this value leads to the best possible condition number provided by the CR based polarimeter (*i.e.*, CN = 2.00). Note that this value is very close to the CN theoretical minimum for polarimetric systems (*i.e.*, $CN_{min} = 1.73$) [11, 12, 42], and thus, it ensures the optimized performance of the CR polarimeter here proposed.

At this point, bearing in mind the discussion related to Figs. 2 and 3, a Quarter-waveplate (QWP) should be chosen to be inserted in the set-up sketched in Fig. 1.

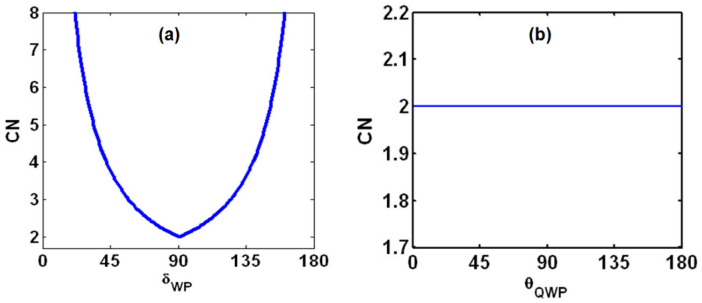

Fig. 3. CN indicator as function of: (a) the WP retardance (and constant $\theta_{WP} = 0°$); (b) the WP orientation (and constant $\delta = 90°$).

Although the CR polarimeter CN does not depend on the WP orientation (see Fig. 2(b) and Fig. 3(b)), the specific Stokes vector variances may be sensitive to this parameter. To obtain higher insight in this issue, the Stokes variances as a function of different QWP orientations are calculated by following Eq. (3). In addition, the EWV indicator is also calculated as the equally weighted addition of the four Stokes element variances. The obtained results are represented in Fig. 4, where the EWV indicator is constant as a function of the QWP orientation (black line). In turn, the *S1* (blue curve) and the *S2* (green curve) variances are dependent on the QWP orientation, compensating their value one to each other, and keeping in this way a constant EWV value.

Therefore, for a general purpose polarimeter which measures a wide variety of Stokes vectors, the QWP orientation is not a significant parameter in terms of optimization (shown by the CN and the EWV indicators). However, if one desires to measure a certain set of Stokes vectors with special interest in some particular Stokes elements, the information provided in Fig. 4 may be of great interest to reduce the variances associated to those specific Stokes elements.

Finally, to study the influence of data redundancy on the CR polarimeter performance, different polarimeters are simulated by changing the number N of Polarization Analyzers (PAs): 8, 12, 20, 100 and 720. Along simulations, the architecture sketched in Fig. 1 was used, where it was considered that a QWP oriented at 0 degrees is placed at the arm 2 (the orientation is arbitrary, as seen in Fig. 3(b)). For each polarimeter simulated, the CN and the EWV indicators were calculated. The obtained CN is equal to 2.00 for all the cases, independently of the N selected. This result was expected as the CN is not sensitive to data redundancy [11]. Regarding to the EWV indicator, the larger the number of PAs used, the smaller the EWV value obtained. In addition, the Stokes variances for different N were

#224967 - $15.00 USD Received 17 Oct 2014; revised 11 Jan 2015; accepted 12 Jan 2015; published 24 Feb 2015

calculated. The obtained results, together with the EWV data, are given in Table 1. The *S1* variance is smaller than the ones for *S2* and *S3* (these last two variances are equal). This particular variances weight distribution is understood by taking into account the data provided in Fig. 4, by bearing in mind that the QWP is oriented at 0 degrees.

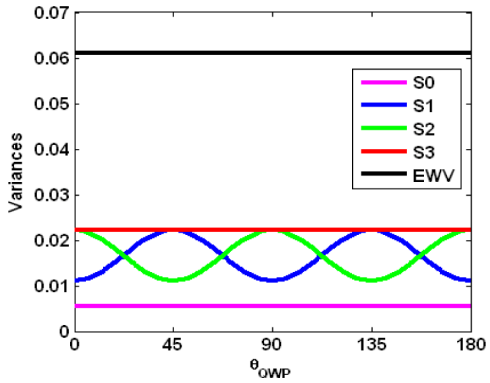

Fig. 4. Equally Weighted Variance (EWV) and Stokes element variances as a function of the QWP orientation (for 720 PAs).

We want to emphasize that the polarimeter architecture proposed in this work leads to a one-shot Stokes polarimeter. This scheme allows us to easily increase the data redundancy just by increasing the number of PAs selected, which can be readily done without an increase of measuring time. This particular characteristic of the CR polarimeter becomes an outstanding feature, in terms of polarimetric metrology.

Table 1. Stokes variances and EWV for the CR based polarimeter when the number of PAs is equal to N = 8, 12, 20, 100 and 720.

Number of PAs	*8*	*12*	*20*	*100*	*720*
S0 variance	0.5000	0.3333	0.2000	0.0400	0.0056
S1 variance	1.0000	0.6667	0.4000	0.0800	0.0111
S2 variance	2.0000	1.3333	0.8000	0.1600	0.0222
S3 variance	2.0000	1.3333	0.8000	0.1600	0.0222
EWV	5.5000	3.6667	2.2000	0.4400	0.0611

4. Robustness and tolerance analysis of the CR polarimeter

In this section, the robustness of the CR polarimeter is studied by simulating deviations from the optimized configuration. Moreover, a tolerance analysis of the parameters involved in the CR polarimeter set-up is conducted as well, being this information of capital importance to evaluate its polarimetric metrology capability and suitability.

4.1 CR based polarimeter robustness

To analyze the robustness of the CR polarimeter, it is considered that the errors associated with the experimental implementation of the polarimeter can be represented by numerical deviations from the optimal Polarization Analyzers (PAs). To this end we performed numerical simulations where random values were added to the Stokes elements that describe each optimal PA of the polarimeter. The random values were taken from a zero mean uniform distribution with 0.4 amplitude (a 20% of the Stokes element values range). The study was conducted both for 32 PAs (*i.e.*, 16 PAs per arm) and for 720 PAs (*i.e.*, 360 PAs per arm). For each case, a total of 50 different polarimeters deviated from the ideal configuration were simulated, and for each one, the corresponding Condition Number (CN) was calculated. The obtained results are given in Fig. 5, where the CN is represented as a function of each one of the 50 different deviated-polarimeters. The results corresponding to 32 PAs and 720 PAs are

#224967 - $15.00 USD Received 17 Oct 2014; revised 11 Jan 2015; accepted 12 Jan 2015; published 24 Feb 2015

represented in Figs. 5(a) and (b), respectively. It is clearly shown that the deviated polarimeters lead to slight modifications of the CN expected (*i.e.*, CN = 2.00). For most applications where polarimetric metrology is required, these small differences are not significant in terms of noise propagation, ensuring the robustness of the CR polarimeter. However, in the case of high-precision polarimetric applications [43], one of the strengths of the CR based polarimeter is highlighted. In fact, as discussed in section 3.2, CR based polarimeters allow to increase the number of PAs selected without increasing the measuring time, leading to more robust configurations (see Fig. 5). Particularly, the standard deviation calculated for CN values given in Fig. 5(a) (32PAs) is of 0.045, whilst for Fig. 5(b) (720PAs) is significantly reduced to 0.009.

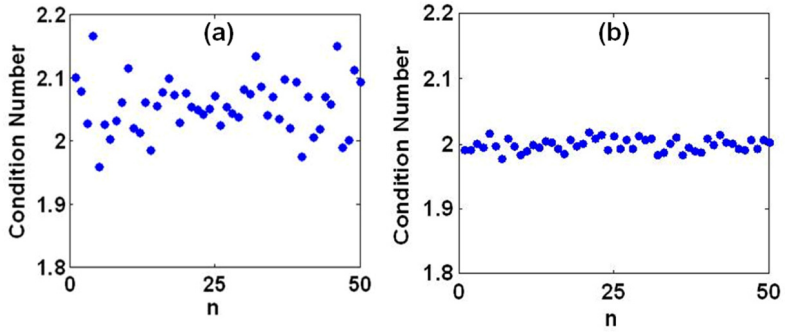

Fig. 5. Condition Number for the 50 different simulated PSAs deviated from the theoretical configuration: (a) for 32 PAs; (b) for 720 PAs.

4.2 CR based polarimeter tolerance

In this section, some features (accuracy-tolerance) related with the design of the CR polarimeter architecture are studied. The accuracy of Stokes polarimeter for a given input polarization is calculated as the largest component of the Stokes vector error (*i.e.*, e_s, see Eq. (5). Here, we study the tolerances for different optical parameters in the set-up when imposing an accuracy of 0.02 in the Stokes vector measurements. Note that accuracy for the Stokes vector in the order of the hundredth is a very suitable value for most polarimetric applications.

To this aim, the error e_s has been evaluated as a function of the incident SoP, as these two factors are strongly related [33, 37]. To homogenously sample the infinite existing fully polarized SoPs, we conduct a parameterization over the Poincaré sphere, given in [37]. The input Stokes vector is expressed as function of its azimuth (θ) and ellipticity (ε), which are parameterized with a variable k:

$$\vec{S}_k = \begin{pmatrix} 1 & \cos 2\theta_k \cos 2\varepsilon_k & \sin 2\theta_k \cos 2\varepsilon_k & \sin 2\varepsilon_k \end{pmatrix}^T$$
$$\begin{cases} \varepsilon_k = k \cdot \Delta\varepsilon - \dfrac{\pi}{4}; \Delta\varepsilon = \dfrac{\pi}{2 \cdot N_\varepsilon \cdot N_\theta} \\ \theta_k = k \cdot \Delta\theta; \Delta\theta = \dfrac{\pi}{N_\theta} \\ k = 1, \ldots, N_\varepsilon \cdot N_\theta \end{cases} \quad (9)$$

In our study, we used N_ε = 20 and N_θ = 50, so in total we have analyzed 1000 different incident Stokes vectors. Four different optical parameters of the CR polarimeter set-up of Fig. 1, susceptible to experimental errors, are studied for different tolerances (deviations in degrees): the orientation and retardance of the QWP (θ_{WP} and δ) and the orientations of the

#224967 - $15.00 USD Received 17 Oct 2014; revised 11 Jan 2015; accepted 12 Jan 2015; published 24 Feb 2015

equivalent polarizers located along the first and second light rings (θ_{P1} and θ_{P2}). Note that the orientations θ_{P1} and θ_{P2} describe, respectively, a rotation in conjunction of the equivalent polarizers located along the first and second rings.

As an example, Fig. 6 shows the obtained Stokes error components as a function of the incident Stokes vector, for a particular tolerance of 1 degree at the analyzed parameters: θ_{WP} in Fig. 6(a), δ in Fig. 6(b), θ_{P1} in Fig. 6(c), and θ_{P2} in Fig. 6(d). Results depicted in Fig. 6 show that Stokes errors related to orientation deviations (see Figs. 6(a), 6(c) and 6(d)) are larger than those associated to the QWP retardance deviations (see Fig. 6(b)). Moreover, whereas largest errors at the *S3* element are related to θ_{WP} (see Fig. 6(a)) and θ_{P2} deviations (see Fig. 6(d)), largest errors at the *S2* element are related to θ_{P1} deviations (see Fig. 6(c)). In addition, errors at the *S1* element are particularly sensitive to θ_{WP}, θ_{P1} and θ_{P2} deviations. Finally, note that *S0* element is the less sensitive to experimental deviations.

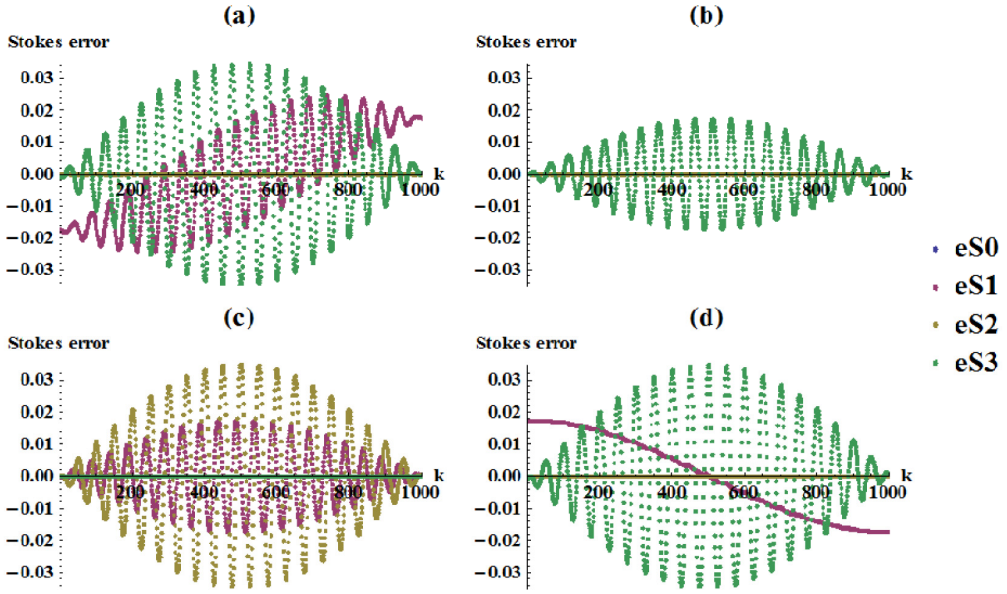

Fig. 6. Stokes elements error for a tolerance of 1 degree at: (a) the QWP orientation (θ_{WP}); (b) the QWP retardance (δ); (c)-(d) the orientations of the equivalents polarizers located along the light rings at the first and second arm (θ_{P1} and θ_{P2}), respectively.

The analysis provided above is repeated for different tolerances: 0.2, 0.5, and 2 degrees. Figure 7 summarizes the results obtained, showing the accuracy of the CR polarimeter as function of the tolerance for the different parameters studied (*i.e.*, θ_{WP}, δ, θ_{P1} and θ_{P2}).

As shown in Fig. 7, the CR based polarimeter accuracy is a linear function of the tolerance, presenting different slopes for the optical parameters analyzed. Thus, a linear fitting is also calculated for each parameter (linear regressions in Fig. 7). In accordance to the results shown in Fig. 6, the accuracy of the polarimetric system is more sensitive to the QWP orientation and to the orientations of the equivalents polarizers along the light rings than to the retardance of the QWP.

At this stage, if an accuracy of 0.02 in the polarization measurements is chosen (red dashed line in Fig. 7) the related tolerances for the four studied parameters are determined. Table 2 shows these calculated tolerances, where the retardance tolerance doubles the other three parameters tolerances.

#224967 - $15.00 USD Received 17 Oct 2014; revised 11 Jan 2015; accepted 12 Jan 2015; published 24 Feb 2015

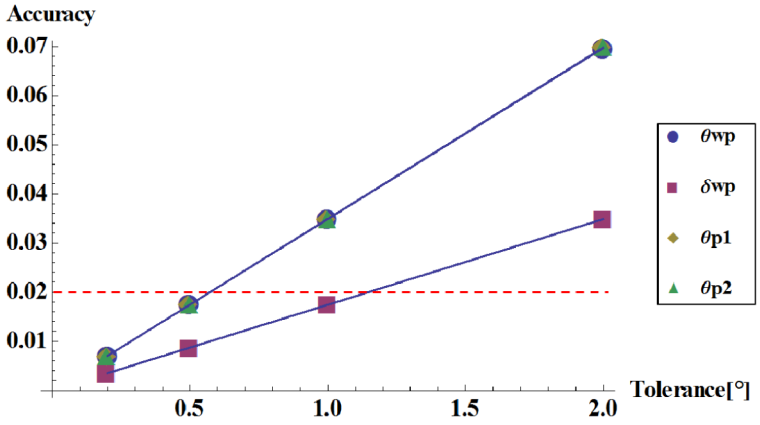

Fig. 7. Accuracy of Stokes polarimeter based on two biaxial crystals as function of the tolerance of different parameters involved in the set-up.

Table 2. Tolerance values to achieve a 0.02 of accuracy in the Stokes polarimeter.

Parameter	θ_{WP}	δ	θ_{LP1}	θ_{LP2}
Tolerance (degrees)	0.57	1.15	0.57	0.57

5. Experimental implementation and results

In this section, the experimental implementation of the CR polarimeter architecture sketched in Fig. 1 is described. In first place we discuss the optimization procedure and different experimental concerns useful to align the set-up. Afterwards, we present the results obtained for different incident SoPs measurements, including fully and partially polarized light.

5.1 CR based polarimeter experimental implementation: optimization and alignment concerns

Following the scheme shown in Fig. 1, the CR polarimeter was implemented. A He-Ne laser (632.8 nm) was used as light source. The B-S used is manufactured by Thorlabs. The two biaxial crystals (BCs) were cut from a monoclinic centro-symmetric $KGd(WO_4)_2$ crystal. Their polished faces (cross-section 6×4 mm^2) have parallelism with less than 10 arcsec, and they are perpendicular to one of the two optic crystal axes within 1.5 mrad misalignment angle. Their lengths, L = 23.38 mm (measured with precision of less than 100 nm), and their conicity, $\alpha = 17$ mrad, provide a CR ring of radius $R_0 = 397$ μm. The BCs were mounted on tip and tilt stages in order to allow the proper alignment to achieve the CR phenomenon. CCD cameras distributed by Basler were used as detectors. We have measured the standard deviation of the background and the maximum value of the ring giving values of 18 and 2924 respectively (*i.e.,* signal to noise ratio equal to 162.4).

The experimental tolerances for the QWP orientation and retardance are 1° and 3°, given by the instrumental error of the optics mount and the manufacturer specifications, respectively. In the case of the tolerances associated to the equivalent polarizers, they depend on the magnification of the imaging system, the pixel size of the camera, and on the radius of the CR ring (R_0). It can be proved that the tolerance of the orientation of the equivalent polarizers is given by $1/N_{pix}$, where N_{pix} is the number of pixels of the radius of the ring on the CCD camera. For the experimental configuration used, a tolerance value of 0.2° is obtained. Note that the experimental tolerances for the WP parameters exceed the values given in Table 2. However, we want to emphasize that by applying an accurate experimental set-up calibration methodology, as those provided in Refs [11, 44], it is possible to experimentally ensure the tolerance conditions given in Table 2, as all the optical elements present in the set-up remain still after calibration.

#224967 - $15.00 USD Received 17 Oct 2014; revised 11 Jan 2015; accepted 12 Jan 2015; published 24 Feb 2015

The independence of the QWP orientation on the CR polarimeter performance was previously discussed in section 3.2, however in that opportunity the beam splitter (B-S) was ideally considered as a non-polarizing element. Experimentally, this approximation may not be valid as the B-S could introduce small values of retardance (different in transmission than in reflection), and so, it would act as a linear retarder. Under this particular scenario, the set conformed by the B-S and the QWP (arm 2 in Fig. 1) would act as an elliptical retarder [9, 45], leading to a behavior slightly different from that represented on the Poincaré sphere in Fig. 2(b), and accordingly, would provide a CN different from the constant shown in Fig. 3(b). As a consequence, the orientation of the QWP could be no longer arbitrary. Consequently, the dependence of the Condition Number (CN) with the QWP orientation was experimentally analyzed. In first place, the Mueller matrix of the B-S was calibrated, both in reflection and in transmission. After conducting the Lu-Chipman decomposition [40, 46], the Jones matrix corresponding to the pure retarder was calculated and finally, the retardance was obtained from their eigenvalues difference. The pure retardances introduced by the B-S due to the birefringence (without taking into account the phase-shift between the two components introduced by reflection) were of −10 and −33 degrees, in transmission and reflection respectively. Thus, by taking into account the experimental Mueller matrix of the B-S, the general expressions given in Eqs. (6) and (7) were applied to the particular experimental set-up implemented in the laboratory. Once the experimental CR polarimeter was characterized, the orientation of the QWP was selected to minimize the CN corresponding to the new PSA configuration. Figure 8 shows the CN results as a function of the QWP orientation. The CN fluctuates from 2.08 to 2.54, values slightly higher than the one obtained when considering the B-S as ideal non-polarizing element (CN = 2.00). Given the two QWP orientations that optimize the PSA configuration (44° and 134°), we have chosen the one corresponding to 44° (marked with a red point in Fig. 8) which provides a minimum CN = 2.08 of the experimental CR polarimeter.

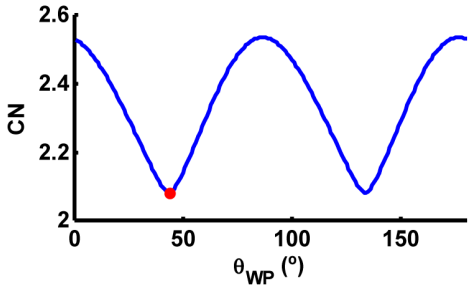

Fig. 8. CN as function of the QWP orientation located at arm 2, considering the experimental B-S Mueller matrix. The red point is marking the minimum CN (2.08), obtained at 44°.

As experimental concerns it should be noted that the focal length of the Lens 0 in Fig. 1 plays an important role in the final intensity ring visualization. It controls the beam waist size (w_0) of the incident beam onto the BC, affecting the CR ring width. In addition, the radius of the CR ring (R_0) at the focal image plane is constant given that it only depends on the length of the crystal and the principal refractive indices [47]. To clearly visualize the CR rings it is necessary to work under conditions of $R_0 >> w_0$, and this is ensured by properly selecting the Lens 0. Besides, as mentioned before, the CR phenomenon is extremely sensitive to the incident angle onto the BC, as this phenomenon is only visible when the incident beam propagates along one of the optic axes of the crystal. Therefore, a very accurate alignment of this element must be conducted.

Note that the WP in Fig. 1 is illuminated with a convergent beam and so, the retardance introduced by this element may be affected by the incident angle. However, by taking into account the size of the experimental light beam (0.1 cm) impinging the convergent lens *L0*

#224967 - $15.00 USD Received 17 Oct 2014; revised 11 Jan 2015; accepted 12 Jan 2015; published 24 Feb 2015

and the focal length of *L0* (*f* = 5 cm), the maximum incident angle on the WP is around 0.6 degrees, leading to a negligible retardance variation for that incident angle.

Last but not least, if a light beam enters into the biaxial crystal with a small angle from its optical axis, although the CR ring is not vanished, some image wander at the CCD plane may occur and should be considered [48]. In our case, we are dealing with a static device, meaning that all the optical elements keep still during polarimetric measurements. However, the required experimental calibration of the polarimeter is based on the use of different known incident SoPs generated by means of an external PSG, including rotating elements. This may lead to small translations on the registered CR rings at the CCD plane. In this situation, if these images had been used to obtain the polarimetric measurement matrix *A* of the system (see Eq. (1)), each pixel would have contained mixed information of different PAs, damaging the calibration. To overcome this problem, a method to center the CR ring was applied. In particular, we centered the acquired images before the calibration calculation. The method is based on the correlation of each acquired image (suffering image wander) with a reference image. This operation gives us the displacement of each individual image with respect to the reference image. Two reference images were used during the image correlation, one for each CCD camera in Fig. 1, because they may have different magnifications. Furthermore, when measuring a given incident SoP, the two acquired images were also correlated with the reference images used in the calibration. This procedure ensures a proper correspondence between the intensity data and the polarimetric measurement matrix, avoiding mismatching between different PAs.

5.2 Polarimetric metrology: experimental results

The performance of the implemented CR polarimeter was tested by measuring different incident SoPs. The number of PAs used per arm was 360, leading to a system with a total of 720 PAs. As first experience, we have generated an array of different fully polarized linear light with variable azimuth. Figure 9(a)-9(c) show, respectively, the azimuth, the ellipticity and the Degree of Polarization (DoP) [40] of the measured SoPs as function of the orientation of the polarizer used for generating the different linear SoPs. The experimental data is represented by blue spots, whilst the red lines describe the theoretical values. An excellent agreement is observed between theoretical and experimental measurements. However, there is a small mismatching for the DoP parameter, as it fluctuates between 0.94 - 1.03 values (*i.e.*, ~0.05 maximum deviation from the theoretical DoP = 1). This small mismatching is originated by different experimental factors, as interferences originated due to back reflections at the optical elements present in the set-up or intensity averages related to the camera pixels size.

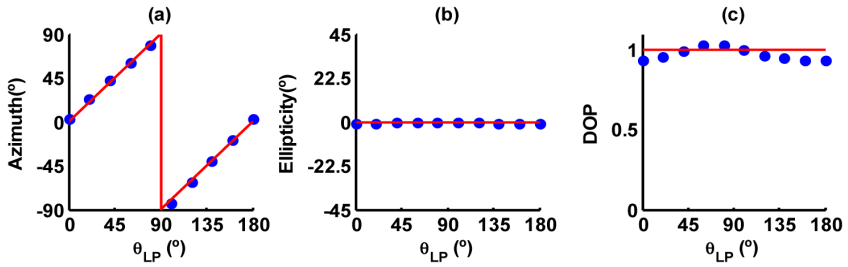

Fig. 9. Fully polarized linear SoP measurements as a function of the polarizer orientation: (a) azimuth, (b) ellipticity and (c) DoP.

Afterwards, the CR polarimeter was tested by measuring incident beams with elliptical polarization. This new set of incident SoPs were generated by means of a rotating linear polarizer, followed by a QWP oriented at 45 degrees. The obtained polarimetric measurements are given in terms of azimuth in Fig. 10(a), of ellipticity in Fig. 10(b) and DoP

#224967 - $15.00 USD Received 17 Oct 2014; revised 11 Jan 2015; accepted 12 Jan 2015; published 24 Feb 2015

in Fig. 10(c). As in the previous case, an excellent agreement between measurements (blue spots) and theoretical values (red lines) is achieved.

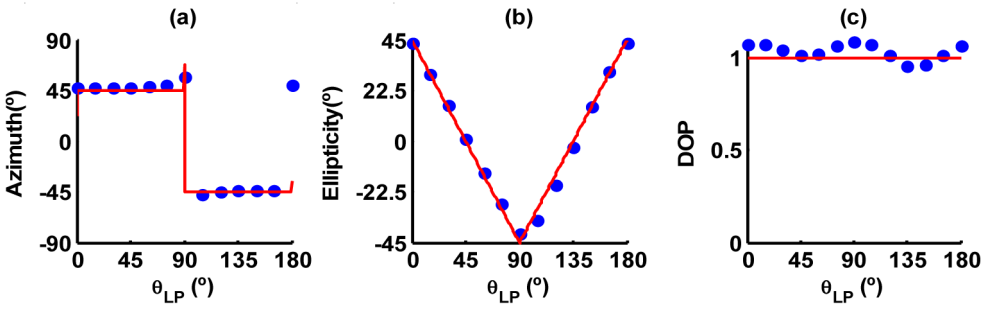

Fig. 10. Fully polarized SoP (with variable ellipticity) measurement, as a function of the polarizer orientation: (a) azimuth, (b) ellipticity and (c) DoP.

Moreover, we have generated partially polarized light with a variable DoP which is controlled by means of a Ferroelectric Liquid Crystal (FLC) cell of nominal retardance λ/2 [49]. By properly aligning the FLC with an incident linear SoP, two orthogonal SoPs can be dynamically generated. When averaging those orthogonal SoPs as a function of time, a SoP with a certain unpolarized content is achieved. A rectangular signal was sent to the FLC to generate these two orthogonal SoPs and, the DoP was controlled by changing the duty cycle (t_1/T) of the rectangular signal sent to the FLC cell, where T is the signal period and t_1 is the part of T in which one of the two selected SoPs is being generated. The obtained results are given in Fig. 11(a)-(c), where respectively the azimuth, ellipticity and DoP parameters are very well determined, as they show a great matching with the simulated values.

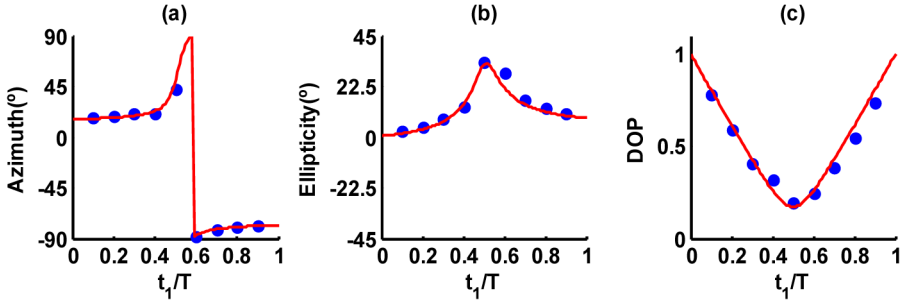

Fig. 11. Partially polarized light, generated by a λ/2 FLC cell when sending a rectangular signal of duty cycle t_1 over a period of T: (a) azimuth, (b) ellipticity and (c) DoP as function of t_1/T.

Summarizing, Figs. 9-11 account for the suitability of the CR based polarimeter to be applied for the measurement of SoPs of fully polarized, partial polarized and fully unpolarized incident light beams. For a higher insight, we have also calculated the Stokes elements error for the three sets of experimental measurements shown in Figs. 9-11. The results are shown, respectively, in Fig. 12(a)-(c). The implemented prototype presents good values of Stokes error. In particular, all errors are smaller than 0.17 (8.5% error, this maximum value is obtained for partially polarized measurements), and in broad terms the most part of the calculated Stokes errors present values lower than 0.1 (5% error). Such performance is suitable for a large number of polarimetry applications providing the interest of the CR polarimeter for polarization metrology. As stated throughout this manuscript, here we present a first experimental prototype of a CR based polarimeter. However, if some possible users require a better accuracy, an accurate alignment protocol ensuring the normal

#224967 - $15.00 USD Received 17 Oct 2014; revised 11 Jan 2015; accepted 12 Jan 2015; published 24 Feb 2015

incidence to the biaxial crystals should be applied, as this is in our opinion the major experimental concern. Despite the above discussion, we think that Stokes errors shown in Fig. 12 are overestimated. This is because results shown in Fig. 12 are the difference between the experimental measurement and the theoretical generated SoP, not the actual generated one.

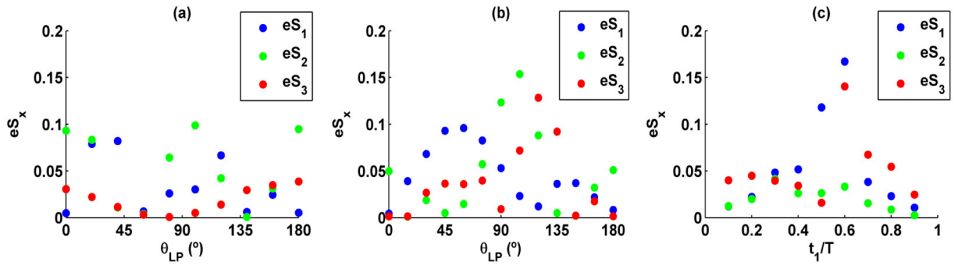

Fig. 12. Stokes elements error for the corresponding sets of experimental measurements: (a) fully polarized linear SoPs (shown in Fig. 9), (b) fully polarized elliptical SoPs (shown in Fig. 10) and (c) partially polarized SoPs (shown in Fig. 11).

7. Conclusion

The concept of a new polarimeter device based on the Conical Refraction (CR) phenomenon was recently introduced in the literature [20]. However, it was not presented a thorough study of its optimization, tolerance analysis, robustness, and experimental implementation. This lack of information, particularly useful for those users interested in the application of CR based polarimeters, has been addressed in this work.

In particular, the optimization of the CR polarimeter performance was conducted by searching the best configuration of optical elements, which was used for the experimental implementation. In addition, a comprehensive study of the robustness and accuracy of CR polarimeters is provided, showing the benefits of including data redundancy to the system, which in these devices can be done without increasing the measuring time.

A CR polarimeter was experimentally implemented and some concerns about the assembling, alignment and calibration are discussed. Finally, the capability of the CR polarimeter was tested by measuring different incident states of polarization, including fully polarized light, partially and fully unpolarized light. The excellent agreement observed between experimental measurements and theoretical prediction validates the suitability of the CR polarimeter to be used for polarimetric metrology.

Acknowledgments

We acknowledge financial support from the Spanish MINECO (FIS2012-39158-C02-01, FIS2011-23719, BES-2010-031696, AP2010-2310 and FEDER) and the Catalan Government (SGR 2014-1639). C. Iemmi thanks the support of UBACyT 20020100100689, CONICET PIP 112-200801-03047, and ANPCYT PICT 2010-02179 (Argentina).

#224967 - $15.00 USD Received 17 Oct 2014; revised 11 Jan 2015; accepted 12 Jan 2015; published 24 Feb 2015